Journal of Materials Chemistry C

Accepted Manuscript

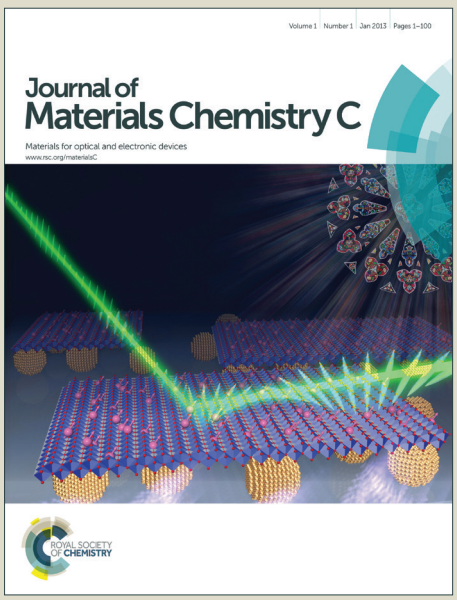

ROYAL SOCIETY OF CHEMISTRY

www.rsc.org/materialsC

Journal of Materials Chemistry C

PAPER

Effective Work Function Modulation of SWCNT-AZO NP Hybrid Electrodes in Fully Solution-Processed Flexible Metal-Oxide Thin Film Transistor

Received 00th January 20xx,
Accepted 00th January 20xx

DOI: 10.1039/x0xx00000x

www.rsc.org/

Su Jeong Lee,[a] Jieun Ko,[b] Jee Ho Park,[a] Jung Han Kim,[c] Gee Sung Chae,[c] Hong Koo Baik,[a] Youn Sang Kim,[b] and Jae-Min Myoung[a*]

The work function modulation of electrode materials is a crucial factor for achieving superior performance in transparent and flexible device applications. In this work, aluminum-doped zinc-oxide nanoparticles (AZO NPs) with a low work function were introduced in single-wall carbon nanotube (SWCNT) transparent electrodes to achieve an Ohmic contact with an indium-oxide (In_2O_3) active layer. These SWCNT-AZO NP hybrid electrodes exhibited a low contact resistance with the solution-processed In_2O_3 active layer, due to the low work function of the AZO NPs physisorbed on the SWCNTs. The 50 nm-thick SWCNT-AZO NP hybrid films showed a considerably low electrical low electrical resistance of 214.5 Ω/sq, an optical transmittance of 82.1% and a work function of 4.57 eV. By using these materials as the source and drain electrodes, fully solution-processed In_2O_3 thin film transistors (TFTs) were fabricated and they showed excellent device performance. Furthermore, the fully solution-processed flexible In_2O_3 TFTs with these SWCNT-AZO NP hybrid electrodes exhibited only a 2.02% decrease in a field effect mobility after 1000 repeated bending stress at a radius of curvature of 3 mm.

Introduction

Research on solution-processed transparent and flexible metal-oxide thin film transistors (TFTs) has been motivated by a variety of device applications, including displays, sensors, solar cells, X-ray detectors, and wearable and imperceptible electronics.[1-6] These applications require materials with superior properties such as flexibility, foldability, deformability, stretchability, and full transparency.[7-11] Specifically, these properties are extremely important to realize flexible and transparent electrodes in order to achieve good device performance.[12] Metal nanowires, metal nanomeshes, metal nanotrough networks, graphene, carbon nanotubes (CNTs), conducting polymer, and composite materials have been widely used for fabricating flexible and transparent electrodes.[12-20] In particular, single-wall carbon nanotubes (SWCNTs) have been considered an attractive material because of their good electrical conductivity, optical transparency, mechanical strength, chemical inertness and high oxidizing temperature.[21-25] However, when the SWCNTs have been used as an electrode material to fabricate metal-oxide TFTs by solution processes, severe contact problems have occurred at the junction between the electrodes and the active layer.[26-28] In most cases, it is due to these SWCNT electrodes have a high work function. Consequently, the electrical performance of the solution-processed metal-oxide TFT degraded. Recently, n-type doped transparent electrodes composed of the SWCNTs and various materials such as alkali metal, ammonia (NH_3), hydrazine, poly(ethyleneimine) (PEI) and benzyl viologen (BV) have been proposed to solve this problem. They have generated a large amount of interest and several results have been reported.[29-36] Nevertheless, these transparent electrodes have low stability under ambient conditions and are not yet compatible in a solution-based device fabrication process.[37,38]

Besides, oxide nanoparticles (NPs) are very interesting additives to SWCNTs for fabricating flexible and transparent electrodes since these NPs are responsible for the electrodes range of work function, transparency and long-term stability. Moreover, a SWCNT-NP solution can be deposited as a uniform film simply by spin coating. By adding oxide NPs with a low work function to the SWCNT electrodes, the work function of the hybrid transparent electrodes can be reduced and an Ohmic contact can be achieved. Accordingly, an efficient carrier injection can be possible at the interface between the hybrid transparent electrodes and the metal-oxide TFT.

[a] Department of Materials Science and Engineering, Yonsei University, 50 Yonsei-ro, Seodaemun-gu, Seoul 120-749, Republic of Korea
[b] . Program in Nano Science and Technology, Graduate School of Convergence Science and Technology, Seoul National University, Seoul 151–744, Republic of Korea
[c] LG Display LCD Research and Development Center, 245 Lg-ro, Wollong-myeon, Paju-si, Gyeonggi-do 413-811, Republic of Korea

†Electronic Supplementary Information (ESI) available: Fig. S1 and Table S1. Electrical characteristics of the TFTs with the AZO NP and the SWCNT-AZO hybrid electrodes as a function of the AZO NPs coating times. Fig. S2 Output characteristics of the TFTs with the SWCNT and the SWCNT-AZO hybrid electrodes. Table S2. Summarized electrical properties of the TFT with the SWCNT and the SWCNT-AZO NP hybrid electrodes and previous results for the TFTs with the SWCNT electrodes. Table S3. Summarized electrical properties of bending cyclic test of the TFT with the SWCNT-AZO NP hybrid electrodes. See DOI: 10.1039/x0xx00000x

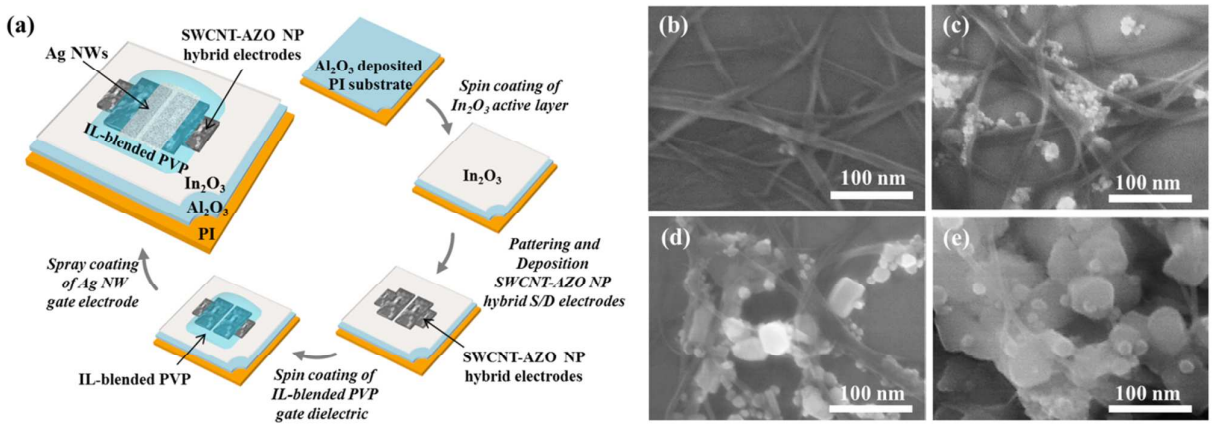

Fig. 1 (a) Schematic diagram of the experimental procedure for the SWCNT-AZO NP hybrid electrode TFT. FE-SEM images of the SWCNT-AZO hybrid films for different number of AZO NP coatings; (b) none, (c) 1, (d) 3 and (e) 5 times.

Therefore, the hybrid transparent electrodes composed of NPs with a lower work function should be studied to improve device performance.

In this report, we have investigated the work function modulation of the SWCNT-aluminum-doped zinc-oxide (AZO) NP hybrid electrodes and their application in solution-processed flexible metal-oxide TFT. By using these electrodes, the optical and electrical properties of the SWCNT electrodes were improved and it is believed that the addition of AZO NPs with a low work function reduced the work function of these hybrid electrodes. These results imply that the SWCNT-AZO NP hybrid electrodes can have a low energy barrier height via a work function modulation and also can enhance the electrical performance of fully solution-processed flexible In_2O_3 TFTs.

Experimental

Preparation and characterization of SWCNT-AZO NP hybrid film

AZO NPs (Sigma-Aldrich) with diameters less than 100 nm were dispersed in deionized (DI) water to prepare a 0.1 wt.% solution by ultrasonication for 2 h. Also, SWCNTs (SA-210, Nano Solution Co. Ltd.) were dispersed in DI water by ultrasonication for 1 h. To promote the dispersion of the SWCNTs solution, sodium dodecyl sulfate (SDS) was added. Prior to the deposition of the SWCNT-AZO NP hybrid film, the SiO_2/p^{++}-Si substrate was cleaned with acetone, methanol and DI water, respectively. The AZO NPs were deposited by spin coating at 2000 rpm for 30 s and where then annealed at 110 °C for 5 min to remove the solvent. In order to control the density of the AZO NPs with the SWCNTs, this coating process was repeated 1, 3 and 5 times. Then, the SWCNT film was deposited on the AZO NP layer by using a spray coating method at 115 °C for a final film thickness of 50 nm. Finally, these SWCNT- AZO NP hybrid films were rinsed with DI water to remove the SDS.

The surface morphologies of the SWCNT and the SWCNT-AZO NP hybrid films were investigated by a field-emission scanning electron microscopy (FESEM, S-5200, HITACHI). The optical properties of the films were evaluated by an ultraviolet-visible spectrophotometer (UV-vis-NIR, V-670, JASCO). The electrical sheet resistances of the films were measured by a four-point probe measurement system (CMT-SR1000N, AiT).

Device fabrication and characterization

The stepwise device fabrication process is depicted in Fig. 1 (a). The metal-oxide TFT with the SWCNT-AZO NP hybrid electrodes was fabricated by the following procedure: A 16 µm-thick polyimide (PI) film substrate was cleaned using acetone, methanol and DI water, respectively. The Al_2O_3 barrier layer was deposited on the PI substrate by an e-beam evaporator and the film thicknesses were fixed at 20 nm. The solution of the In_2O_3 precursor was synthesized by a sol-gel method using 0.1 M indium nitrate hydrate ($In(NO_3)_3 \bullet xH_2O$, Sigma-Aldrich) in DI water. After the solution was vigorously stirred for 24 h, this solution was filtered through a 0.2 µm polytetrafluoroethylene (PTFE) syringe filter. Then, this filtered solution was spin-coated on the Al_2O_3/PI substrate at 3000 rpm for 20 s. The In_2O_3 active layer with a thickness of 7 nm was formed and annealed at 250 °C for 1.5 h. Following the photo-lithography and lift-off process, the source and drain electrodes of the SWCNT and SWCNT-AZO NP hybrid films were deposited on the In_2O_3/Al_2O_3/PI substrate.[27]

To synthesize the ionic liquid-blended polyvinylphenol (IL-blended PVP) dielectric layer, a 15 wt.% PVP solution, composed of polyvinylphenol (poly(4-vinylphenol), Sigma-Aldrich), 4,4'-(hexafluoroisopropylidene diphthalic anhydride) (HDA) and propylene glycol monomethyl ether acetate (PGMEA), was stirred for 12 h. Then, this solution was mixed with a few drops of 1-ethyl-3-methylimidazolium bis(trifluoromethylsulfonyl)imide (EMIM-TFSI), an ionic liquid. After the solution was filtered through a 0.2 µm PTFE syringe filter, the filtrate was spin-coated on the SWCNT-AZO NP/In_2O_3/Al_2O_3/PI substrate at 2000 rpm for 30 s. Subsequently, it was annealed at 70 °C for 12 h in a vacuum oven. To ensure adequate film hardness, a post-annealing

Fig. 2 Transmittance versus sheet resistance of (a) the SWCNT films as a function of thickness and (b) the 50 nm-thick SWCNT-AZO NP hybrid films for different number of AZO NP coatings.

process was performed at 110 °C for 1 h. Finally, the top gate electrode of the Ag NW film with a thickness of 100 nm was deposited by spray coating through a shadow mask at 120 °C.[39] The work functions of the In_2O_3, SWCNTs, AZO NPs and SWCNT-AZO NPs were measured by a surface analyzer photoelectron spectrometer (AC-2, Riken Keiki Co. Ltd). The electrical properties of the TFTs with the SWCNT and the SWCNT-AZO NP hybrid electrodes were measured by a semiconductor parameter analyzer system (Agilent B1500A, Agilent Technologies). Also, these devices were measured in ambient conditions without any device encapsulation.

Results and discussion

In order to control the density of the AZO NPs with the SWCNT film, the number of spin-coating of AZO NP solution was varied. Fig. 1 (b)-(e) show the top-view FE-SEM images of the SWCNT-AZO NP hybrid films for different number of AZO NP coatings. Fig. 1 (b) clearly shows that the SWCNT film with the intrinsic random networks was deposited. Increasing the number of coatings considerably increased the effective contact area between the SWCNTs and the AZO NPs, as shown in Fig. 1 (c)-(e). This results in an increase in the effective conducting pathways of the SWCNTs with the AZO NPs and the effective contact area of the AZO NPs with the In_2O_3 active layer. The surface morphology of the most uniform physisorbed condition was obtained after spin coating the AZO NP 3 times, as shown in Fig. 1 (d). However, further coatings led to the aggregation of the AZO NPs, as shown in Fig. 1 (e).

Table 1 Summarized work functions of the AZO NPs, SWCNTs, SWCNT-AZO NP hybrid and In_2O_3 layers.

	Materials	Work function (eV)
SWCNT-AZO NP hybrid	AZO NPs	4.32
	SWCNTs	4.96
	1 time of the AZO NP coating	4.79
	3 times of the AZO NP coating	4.57
	5 times of the AZO NP coating	4.54
	In_2O_3	4.61

Fig. 2 shows the transmittance and the sheet resistance of the SWCNT and SWCNT-AZO NP hybrid films. For the SWCNT films shown in Fig. 2 (a), as the film thickness increased from 25 to 250 nm, the sheet resistance decreased from 2289.8 to 121.86 Ω/sq and the optical transmittance decreased from 94.45 to 52.18%, respectively. However, for the 50 nm-thick SWCNT-AZO NP hybrid films, as the number of coatings increased, the optical transmittances remained between 84.77 and 81.67%, as shown in Fig. 2 (b). Moreover, the sheet resistance decreased rapidly from 1086.6 to 214.5 Ω/sq after 3 AZO NP coatings. However, with a further increase in the number of the AZO NP coatings, the sheet resistance increased gradually due to the aggregation of the AZO NPs, which interfered with smooth carrier movement.

The work functions of the AZO NPs, SWCNTs and In_2O_3 layer were obtained as 4.32, 4.96 and 4.61 eV, respectively (Table 1). Moreover, with increasing AZO NP coating times from 1 through 3 to 5, the work function of the SWCNT-AZO NP hybrid layer decreased from 4.79 through 4.57 to 4.54 eV. One interesting thing is that, although AZO NP coating times increased from 3 to 5, the change of the work function was very small (~0.03 eV). So, when considering that the surface morphology of the most uniform physisorbed condition is obtained after 3 AZO NP coatings (Fig. 1 (d)), the optimum AZO NP coating times is determined to be 3 and this condition is fixed for this research. Using these values, schematic energy band diagrams at the junctions between the SWCNT electrodes and the In_2O_3 active layer and between the SWCNT-AZO NP hybrid electrodes and the In_2O_3 active layer were induced, as shown in Fig. 3 (a). When the SWCNT electrodes are brought into direct contact with the In_2O_3 active layer, a Schottky carrier injection barrier is formed with a barrier height of 0.35 eV. In contrast, when the SWCNT-AZO NP hybrid electrodes are brought into direct contact with the In_2O_3 active layer, an Ohmic contact is formed. The conventional SWCNTs with the inert graphitic chemical structure suffer from difficulties in work function modulation. However, physisorption of the AZO NPs on SWCNTs leads to work function modulation of the SWCNTs due to the low work function of the AZO NPs. Thus, the work function of the

SWCNT-AZO NP hybrid film decreased to 4.57 eV, resulting in an Ohmic contact.

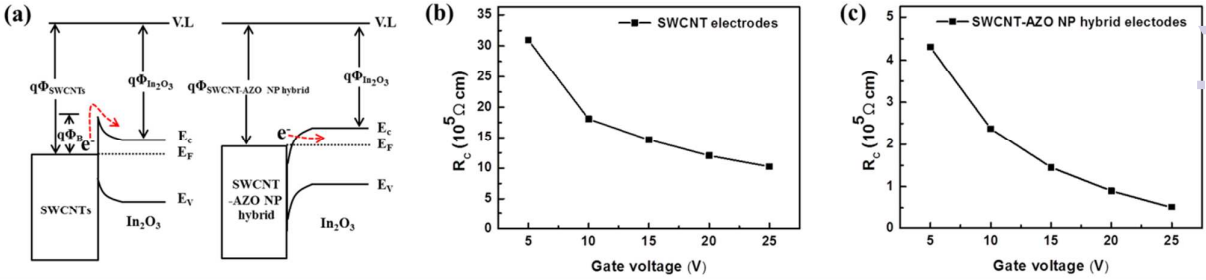

Fig. 3 (a) Schematic energy band diagrams at the junctions of the SWCNT electrodes/In_2O_3 active layer and the SWCNT-AZO NP hybrid electrodes/In_2O_3 active layer. Electrical contact resistance of the TFTs with (b) the SWCNT and (c) the SWCNT-AZO NP hybrid electrodes as a function of gate voltage.

Electrical properties of the contact resistance were evaluated by using the transmission line method (TLM) and the following equations:[40,41]

$$R_T = V_{DS} + I_{DS} = R_{ch}L + R_{SD}(= 2R_{S/D}), \quad (1)$$

$$L_T = R_{S/D} / R_{Ceff}, \quad (2)$$

$$R_{Ceff} = WL_T^2 R_{ch} = WR_{S/D}^2 / R_{ch}, \quad (3)$$

$$R_C = R_{SD} L_T W, \quad (4)$$

Where R_T, R_{ch}, L, R_{SD} and $R_{S/D}$ are the total TFT ON resistance, the channel resistance per unit channel length, the physical channel length, the series resistance at the source/drain contacts and the series resistance at the source or drain contact, respectively. In addition, L_T and R_{Ceff} are respectively the effective transfer length and the effective contact resistance. The TLM patterns were formed by coating SWCNT electrodes or SWCNT-AZO NP hybrid electrodes, respectively, on the structure of In_2O_3/300 nm-thick SiO_2/p^{++}-Si. The channel width was 400 μm and the channel lengths were controlled to be 50, 100, 150, 200 and 250 μm, respectively.

Fig. 3 (b) and (c) show the contact resistance as a function of the gate voltage for the SWCNT electrodes and the SWCNT-AZO hybrid electrodes on the In_2O_3 active layer. As shown in Fig. 3 (b), the contact resistance (R_C) of the TFT with the SWCNT electrodes was changed from 3.09 to 1.02 MΩ by varying the gate voltages (V_{GS}) from 5 to 25 V in 5 V steps. For the TFT with the SWCNT-AZO NP hybrid electrodes, the R_C was changed from 430.6 to 50.6 kΩ with the same V_{GS} conditions as shown in Fig. 3 (c). The R_C values of the TFTs with the SWCNT and the SWCNT-AZO NP hybrid electrodes decreased as V_{GS} increased. Most significantly, however, the R_C values of the TFTs with the SWCNT-AZO NP hybrid electrodes were one order of magnitude lower than those of the TFTs with the SWCNT electrodes. This result evidently implies that the energy barrier height between the SWCNT-AZO hybrid electrodes and the In_2O_3 active layer was reduced compared to that between the SWCNT electrodes and the In_2O_3 layer.

In order to investigate the effects of the SWCNT-AZO NP hybrid electrodes on the fully solution-processed flexible TFT, TFTs with SWCNT and SWCNT-AZO NP hybrid electrodes were prepared on 300 nm-thick SiO_2/p^{++}-Si and PI substrates, respectively. Fig. 4 (a) shows a photograph of a top gate-type TFT with a coplanar structure (the Ag NW/IL-blended PVP/SWCNT-AZO NP hybrid/In_2O_3/Al_2O_3/PI). The thicknesses of the Ag NW, SWCNT-AZO NP hybrid, In_2O_3, and IL-blended PVP layers were 100, 50, 7 nm and 1 μm, respectively. The channel width and length were 1000 and 200 μm, respectively. Fig. 4 (b)-(d) show the transfer characteristics of the TFTs with the SWCNT and the SWCNT-AZO NP hybrid electrodes. The electrical properties of all devices are summarized in Table 2.

The SWCNT electrode TFT on the SiO_2/p^{++}-Si substrate showed a sub-threshold slope (S.S) of 6.59 V/decade, a threshold voltage (V_{th}) of 3.02 V, a field-effect mobility (μ_e) of 2.65 $cm^2/V{\cdot}s$ and an on/off current ratio (I_{on}/I_{off}) of 6.75×10^2 at a V_D of 20 V. Meanwhile, the SWCNT-AZO NP hybrid electrode TFT on the SiO_2/p^{++}-Si exhibited a S.S of 3.34 V/decade, a V_{th} of 1.92 V, a μ_e of 5.14 $cm^2/V{\cdot}s$ and an I_{on}/I_{off} of 8.15×10^3 at a V_D of 20 V (Fig. 4 (b)).

For comparison, the electrical characteristics of the TFTs with the AZO NP electrodes and the SWCNT-AZO NP hybrid electrodes as a function of the AZO NPs coating times are

Journal of Materials Chemistry C

PAPER

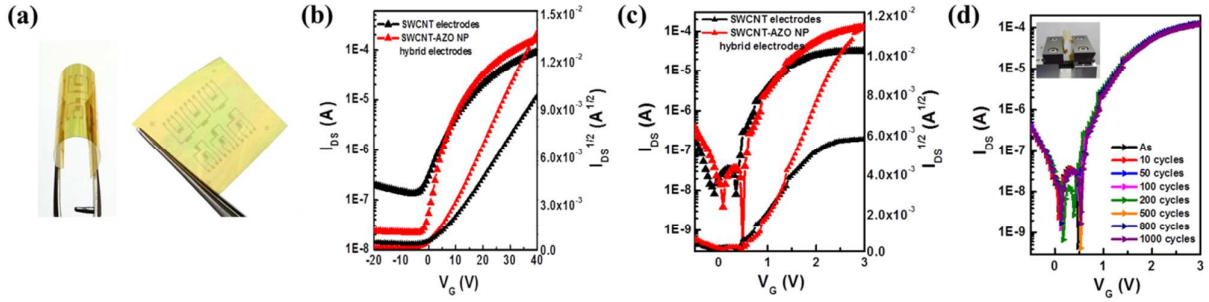

Fig. 4 Electrical characteristics of the TFTs with the SWCNT electrodes and the SWCNT-AZO NP hybrid electrodes. (a) Optical image of the TFT with the SWCNT/AZO NP hybrid electrodes on PI substrate, (b) transfer characteristics with a V_D of 20 V on SiO_2/p^{++}-Si substrate, (c) transfer characteristics with a V_D of 1 V on PI substrate and (d) transfer characteristics of the TFT with the SWCNT-AZO NP hybrid electrodes on PI substrate after 1000 cycles of bending test at the radius of curvature of 3 mm.

Table 2 Summarized electrical properties of the TFT with the SWCNT electrodes and the SWCNT-AZO NP hybrid electrodes.

TFT Structure	Sub-threshold slope (V/decade)	Threshold voltage (V)	Field-effect mobility ($cm^2/V{\cdot}s$)	On/off current ratio
SWCNT/$In_2O_3/SiO_2/p^{++}$-Si	6.59	3.02	2.65	6.75×10^2
SWCNT-AZO NP hybrid/$In_2O_3/SiO_2/p^{++}$-Si	3.34	1.92	5.14	8.15×10^3
Ag NW/IL- blended PVP/SWCNT/In_2O_3/Al_2O_3/PI	0.08	0.49	2.14	3.24×10^3
Ag NW/IL- blended PVP/SWCNT-AZO NP hybrid/In_2O_3/Al_2O_3/PI **(Before bending)**	0.05	0.75	5.44	3.71×10^4
Ag NW/IL- blended PVP/SWCNT-AZO NP hybrid/In_2O_3/Al_2O_3/PI **(After 1000 bending cycles)**	0.05	0.80	5.33	6.02×10^4

shown in Fig. S1 and Table S1. In this work, the TFT with AZO NP electrodes did not work because the sheet resistance of the AZO NPs is too high. However, when changing the number of the AZO NP coatings up to 5 times, the TFT with the SWCNT-AZO NP hybrid electrodes coated 3 times exhibited the best electrical properties.

When the PI substrate was used with the SWCNT electrodes, the TFT showed a S.S of 0.08 V/decade, a V_{th} of 0.49 V, a μ_e of 2.14 $cm^2/V{\cdot}s$ and an I_{on}/I_{off} of 3.24×10^3 at V_D of 1 V. However, the TFTs with the SWCNT-AZO NP hybrid electrodes exhibited a S.S of 0.05 V/decade, a V_{th} of 0.75 V, a μ_e of 5.44 $cm^2/V{\cdot}s$ and an I_{on}/I_{off} of 3.71×10^4 at a V_D of 1 V (Fig. 4 (c)). Regardless of the substrate, the TFTs with the SWCNT-AZO NP hybrid electrodes demonstrated much better electrical properties than those with the SWCNT electrodes.

Also, this flexible device showed better electrical properties when compared to our previous results in Table S2.

Fig. S2 shows the output characteristics of the TFTs with the SWCNT and the SWCNT-AZO NP hybrid electrodes as the V_{GS} varied from 0 to 2 V in 0.4 V steps. The current-voltage characteristics of the TFTs with the SWCNT electrodes at low source-drain voltages exhibit the non-linear behavior of a non-Ohmic contact, as highlighted with a red circle in Fig. S2 (a). However, the TFTs with the SWCNT-AZO NP hybrid electrodes at low source-drain voltages show the linear output behavior of an ideal Ohmic contact, as highlighted with a red circle in Fig. S2 (b).[42] It is due to AZO NPs have a lower work function than that of the SWCNTs. As a result, the smooth movement of the carrier and the enhancement of device performance in the TFTs with the SWCNT-AZO NP hybrid electrodes were possible.

Fig. 4 (d) shows the transfer characteristics of the fully solution-processed TFTs with SWCNT-AZO NP hybrid electrodes on a PI substrate, after 1000 cycles of a bending test with a radius of curvature of 3 mm. This TFT exhibited only slight degradation in a field-effect mobility from 5.44 to 5.33 $cm^2/V{\cdot}s$. Moreover, it is notable that this device was still functional after 1000 cycles, suggesting stable reliability with respect to the repeated bending stress (Table S3). These results clearly demonstrate that the presence of the AZO NPs induced the work function modulation through robust

physisorption to the SWCNTs. Furthermore, the SWCNT-AZO NP hybrid film can be used as flexible and transparent electrodes for the high-performance solution-processed TFTs.

Conclusions

In summary, we reported that work function modulation of the SWCNT-AZO NP hybrid electrodes was achieved by adding AZO NPs to the SWCNTs. This is a result of the low work function of AZO NPs relative to that of the SWCNTs. Consequently, the energy barrier height and contact resistance at the junction between the hybrid electrodes and the In_2O_3 active layer were reduced to form an Ohmic contact. When these hybrid electrodes were used on fully solution-processed TFTs with a structure of the Ag NW/IL-blended PVP/SWCNT-AZO NP hybrid/In_2O_3/Al_2O_3/PI, a S.S of 0.05 V/decade, a V_{th} of 0.75 V, a μ_e of 5.44 $cm^2/V{\cdot}s$ and an I_{on}/I_{off} of 3.71×10^4 were obtained. Moreover, the field effect mobility of the device was decreased by only 2.02% after a 1000 repeated bending stress. Therefore, it is believed that these SWCNT-AZO NP hybrid electrodes are an excellent electrode material candidate for the high-performance, transparent and flexible devices fabricated by full solution processes.

Acknowledgements

This work was supported by the IT R&D program of MOTIE/KEIT (No. 10042414, Development of 8th Generation (2200×2500 mm^2) Major Equipment for Transparent Flexible Display in Large Area) and by the LG Display Academic Industrial Cooperation Program (No. 2013-11-2012).

Notes and references

1 A. Facchetti, and T. J. Marks, *Transparent Electronics*, John Wiley & Sons, West Sussex, United Kingdom, 2010.
2 K.-H. Lee, S.-M. Kim, H. Jeong, Y. Pak, H. Song, J. Park, K.-H. Lim, J.-H. Kim, Y. S. Kim, H. C. Ko, I. K. Kwon and G.-Y. Jung, *Adv. Mater.*, 2013, **25**, 3209.
3 Y. Sun and J. A. Rogers, *Adv. Mater.*, 2007, **19**, 1897.
4 A. C. Arias, J. D. MacKenzie, I. McCulloch, J. Rivnay and A. Salleo, *Chem. Rev.*, 2010, **110**, 3.
5 S. R. Thomas, P. Pattanasattayavong and T. D. Anthopoulos, *Chem. Soc. Rev.*, 2013, **42**, 6910.
6 S. Jeong and J. Moon, *J. Mater. Chem.*, 2012, **22**, 1243.
7 J.-Y. Sun, N. Lu, J. Yoon and K.-H. Oh, *J. Mater. Res.*, 2009, **24**, 3338.
8 Z. Liu, J. Xu, D. Chen and G. Shen, *Chem. Soc. Rev.*, 2015, **44**, 161.
9 D.-H. Kim, J. Xiao, J. Song, Y. Huang and J. A. Rogers, *Adv. Mater.*, 2010, **22**, 2108.
10 K. Kim, E. Lee, J. kim, S. Y. Park, K.-H. Lim, C. H. Shin and Y. S. Kim, *J. Mater. Chem. C*, 2013, 1, 7742.
11 D. S. Hecht, L.Hu and G. Irvin, *Adv.Mater.*, 2011, **23**, 1482.
12 L. Hu, H. Wu and Y. Cui, *MRS Bull.*, 2011, **36**, 760.
13 Z. Yin, C. Lee, S. Cho, J. Yoo, Y. Piao, and Y. S. Kim, *Small*, 2014, **10**, 5047.
14 C.-H. Liu and X. Yu, *Nanoscale Res. Lett.*, 2011, **6**, 75.
15 H.-Z. Geng, K. K. Kim, K. P. So, Y. S. Lee, Y. Chang and Y. H. Lee, *J. Am. Chem. Soc.*, 2007, **129**, 7758.
16 W. H. Lee, J. Park, S. H. Sim, S. B. Jo, K. S. Kim, B. H. Hong and K. Cho, *Adv. Mater.*, 2011, **23**, 1752.
17 H. D. Tran, D. Li and R. B. Kaner, *Adv. Mater.*, 2009, **21**, 1487.
18 C. F. Guo, Y. Lan,.T. Sun and Z. Ren, *Nano Energy*, 2014, **8**, 110.
19 H.-J. Kim, S.-H. Lee, J. Lee, E.-S. Lee, J.-H. Choi, J.-Ho Jung, J.-Y. Jung and D.-G. Choi, *Small*, 2014, **10**, 3767.
20 T. He, A. Xie, D. H. Reneker and Y. Zhu, *ACS Nano*, 2014, **8**, 4282.
21 R. L. McCreery, *Chem. Rev.*, 2008, **108**, 2646.
22 G. Gruner, *J. Mater.Chem.,* 2006, **16**, 3533.
23 R. S. Ruoff, D. Qian and W. K. Liu, *C. R. Phys.*, 2003, **4**, 993.
24 D. Tasis, N. Tagmatarchis, A. Bianco and M. Prato, *Chem. Rev.*, 2006, **106**, 1105.
25 V. Sgobba and D. M. Guldi, *Chem. Soc. Rev.*, 2009, **38**, 165.
26 J. Jeon, T. I. Lee, J. H. Choi, J. P. Kar, W. J. Choi, H. K. Baik, J. M. Myoung, *Electrochem. Solid-State Lett.*, 2011, **14**, H76.
27 J. H. Park, S. J. Lee, T. I. Lee, J. H. Kim, C. H. Kim, G. S. Chae, M. H. Ham, H. K. Baik and J. M. Myoung, *J. Mater. Chem. C*, 2013, **1**, 1840.
28 S. J. Lee, T. I. Lee, J. H. Park, I.-K. Oh, H. Kim, J. H. Kim, C.-H. Kim, G. S. Chae, H. K. Baik and J.-M. Myoung, *J. Mater. Chem. C*, 2015, **3**, 1403.
29 P. Qi, O. Vermesh, M. Grecu, A. Javey, Q. Wang and H. Dai, *Nano Lett.*, 2003, **3**, 347.
30 B. H. Kim, T. H. Park, S. J. Baek, D. S. Lee, S. J. Park, J. S. Kim and Y. W. Park, *Appl. Phys. Lett.*, 2008, **103**, 096103.
31 K. S. Mistry, B. A. Larsen, J. D. Bergeson, T. M. Barnes, G. Teeter, C. Engtrakul and J. L. Blackburn, *ACS Nano*, 2011, **5**, 3714.
32 S. M. Kim, J. H. Jang, K. K. Kim, H. K. Park, J. J. Bae, W. J. Yu, I. H. Lee, G. Kim, D. D. Loc, U. J. Kim, E.-H. Lee, H.-J. Shin, J.-Y. Choi and Y. H. Lee, *J. Am. Chem. Soc.*, 2009, **131**, 327.
33 M. Shim, A. Javey, N. W. S. Kam and H. Dai, *J. Am. Chem. Soc.*, 2001, **123**, 11512.
34 C. Jiang, A. Saha, C. Xiang, C. C. Young, J. M. Tour, M. Pasquali and A. A. Martí, *ACS Nano*, 2013, **7**, 4503.
35 C. Jiang, A. Saha, C. C. Young, D. P. Hashim, C. E. Ramirez, P. M. Ajayan, M. Pasquali and A. A. Martí, *ACS Nano*, 2014, **8**, 9107.
36 A. Pe´nicaud, P. Poulin, A. Derre´, E. Anglaret and P. Petit, *J. Am. Chem. Soc.*, 2005, **127**, 8.
37 R. S. Lee, H. J. Kim, J. E. Fischer, A. Thess and R. E. Smalley, *Nature*, 1997, **388**, 255.
38 C. Wang, K. Ryu, A. Badmaev, J. Zhang and C. Zhou, *ACS Nano*, 2011, **5**, 1147.
39 J. Ko, S. J. Lee, K. Kim, E. Lee, K.-H. Lim, J.-M. Myoung, J. Yoo and Y. S. Kim, *J. Mater. Chem. C*, 2015, **3**, 4239.
40 C. R. Kagan and P. Andry, *Thin-Film Transistors*, Marcel Dekker, Inc., 2003.
41 J. Park, C. Kim, S. Kim, I. Song, S. Kim, D. Kang, H. Lim, H. Yin, R. Jung, E. Lee, J. Lee, K.-W. Kwon and Y. Park, *IEEE Electron Device Lett.*, 2008, **29**, 879.
42 G. B. Blanchet, C. R. Fincher, M. Lefenfeld and J. A. Rogers, *Appl. Phys. Lett.*, 2004, **84**, 296.

Graphical abstract

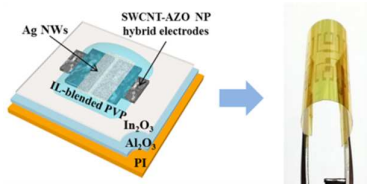

Schematic diagram of the SWCNT-AZO NP hybrid electrode TFT and the optical image of the TFT with the SWCNT/AZO NP hybrid electrodes on PI substrate.